PLOS ONE

RESEARCH ARTICLE

Dynamic Impedance Model of the Skin-Electrode Interface for Transcutaneous Electrical Stimulation

José Luis Vargas Luna[1,2]*, Matthias Krenn[3], Jorge Armando Cortés Ramírez[2], Winfried Mayr[3]

1 Health Technology Center, Reykjavik University / Landspitali—University Hospital, Reykjavik, Iceland, **2** Escuela de Ingeniería y Ciencias, Tecnológico de Monterrey, Monterrey, Nuevo León, Mexico, **3** Center of Medical Physics and Biomedical Engineering, Medical University of Vienna, Vienna, Austria

* joseluis.vargasluna@gmail.com

CrossMark
click for updates

OPEN ACCESS

Citation: Vargas Luna JL, Krenn M, Cortés Ramírez JA, Mayr W (2015) Dynamic Impedance Model of the Skin-Electrode Interface for Transcutaneous Electrical Stimulation. PLoS ONE 10(5): e0125609. doi:10.1371/journal.pone.0125609

Academic Editor: Mikhail A. Lebedev, Duke University, UNITED STATES

Received: December 22, 2014

Accepted: March 24, 2015

Published: May 5, 2015

Copyright: © 2015 Vargas Luna et al. This is an open access article distributed under the terms of the Creative Commons Attribution License, which permits unrestricted use, distribution, and reproduction in any medium, provided the original author and source are credited.

Data Availability Statement: All relevant data are available from Figshare, at the following URL: http://figshare.com/s/d4d66790d93d11e4ae9206ec4bbcf141.

Funding: This work was supported by the Vienna Science and Technology Fund (WWTF), Proj.Nr. LS11-057 (www.wwtf.at), and the Wings for Life Spinal Cord Research Foundation (WfL), Proj.Nr. WFL-AT-007/11 (http://www.wingsforlife.com) The funders had no role in study design, data collection and analysis, decision to publish, or preparation of the manuscript.

Abstract

Transcutaneous electrical stimulation can depolarize nerve or muscle cells applying impulses through electrodes attached on the skin. For these applications, the electrode-skin impedance is an important factor which influences effectiveness. Various models describe the interface using constant or current-depending resistive-capacitive equivalent circuit. Here, we develop a dynamic impedance model valid for a wide range stimulation intensities. The model considers electroporation and charge-dependent effects to describe the impedance variation, which allows to describe high-charge pulses. The parameters were adjusted based on rectangular, biphasic stimulation pulses generated by a stimulator, providing optionally current or voltage-controlled impulses, and applied through electrodes of different sizes. Both control methods deliver a different electrical field to the tissue, which is constant throughout the impulse duration for current-controlled mode or have a very current peak for voltage-controlled. The results show a predominant dependence in the current intensity in the case of both stimulation techniques that allows to keep a simple model. A verification simulation using the proposed dynamic model shows coefficient of determination of around 0.99 in both stimulation types. The presented method for fitting electrode-skin impedance can be simple extended to other stimulation waveforms and electrode configuration. Therefore, it can be embedded in optimization algorithms for designing electrical stimulation applications even for pulses with high charges and high current spikes.

Introduction

Electrical stimulation is a powerful tool for diagnosis, treatment and function restoration in the human body. When applied transcutaneously, the impedance of the skin-electrode interface should be carefully considered, since previous reports have shown that it has a non-negligible direct influence on the stimulation outcome [1].

Competing Interests: The authors have declared that no competing interests exist.

Many studies have reported spectroscopy measurements of tissue-electrode impedance, deriving mathematical models mainly on basis of electrical resistive-capacitive (RC) equivalent circuits or networks [2–5]. However, these spectroscopy models are based on recordings with sinusoidal low amplitudes currents, whereas clinical or research applications rely on impulse currents and much higher intensity levels. Typical electrical stimulation therapies use rectangular or triangular pulses at relatively low frequencies (<50Hz), and pulse widths of <2000μs for nerve and neuromuscular stimulation [6] or >30ms for denervated muscles [7]. Only few studies are found that focus directly on impedance dynamics under transcutaneous electrical stimulation and, most of them, only consider low-charge pulses [8,9]. It has been reported that current-voltage response on long pulses differ quite significantly from a behavior to be expected from conventional models based on fixed (within pulses) RC networks [10,11].

The better understanding of the skin-electrode interface impedance and the ability to predict its behavior under typical electrical stimulation conditions is important, since previous studies suggest that the impedance plays an important role for the performance and controllability of current-controlled (CC) and voltage-controlled (VC) stimulation [1]. Moreover, new approaches for improvements in selectivity of stimulation are based on novel shapes of stimulation waveforms. For example, it has been reported that the use of depolarizing pre-pulses can reduce fiber excitability [12], while hyperpolarizing pre-pulses can increase it [13]. Stimulus waveforms that include such pre-pulses work at low as well as at high intensities, therefore understanding the underlying mechanisms acting within the skin-electrode interface could be a key factor for development of new devices and stimulus designs.

Preliminary reports have showed that it is possible to develop a well correlating model of the skin-electrode interface impedance during application of typical transcutaneous electrical stimulation pulses [11] valid for both low and high impulse charges. The main aim of this work is to provide extended systematic experimental data on application of CC and VC biphasic rectangular stimuli via electrodes of various sizes and associated model calculations that allow to some extend general predictive calculations for other stimulus shapes and stimulation setups.

Methodology

To understand observed impedance variations during transcutaneous electrical stimulation better, it is necessary to recognize influences of skin anatomy and electrical properties of its structures. Based on a literature study, a mathematical model that considers known mechanisms was developed that can be easily implemented in simulations. Further an experimental setup was defined to acquire data for calculating the variables of the model. Finally, the model is validated with simulation with different impulses shapes and the accuracy is discussed.

Skin properties

The skin is a complex structure, but essentially composed by two layers: the epidermis (outer layer) and the dermis. Together they can vary in thickness depending on the body region, from 0.5mm at the eyelid up to more than 4mm at the foot sole.

The epidermis is composed principally of keratinocytes (~90%), melanocytes, Langerhans cells and Merkel cells [14]. It is, in general sense, a lipid-corneocyte matrix arranged in a flattened and irregular fashion [15], which is crossed by skin appendages (*e.g.* sweat glands and hair follicles) [16]. The outer layer of the epidermis is called *stratum corneum*. It is composed by a lipid lamellae-corneocyte matrix arranged in bilayers (between 25 and 100) and has an approximate thickness between 10 to 100μm [14,17,18].

The dermis is mainly composed by connective tissue (collagen and elastic fibers), but also fibroblast, macrophages and adipocytes [14]. It also has a great density of blood vessels [15],

lymphatic vessels, sensory receptors, related nerves and glands [19], and follicles. The skin appendages density may vary upon the region of the skin. The sweat glands, for example, have a density between 1–6 pores/mm^2 [14,15,20].

The dermis tissue, as well as deeper structures, has a stable environment that is rich in ions, which provides low and stable impedance levels. On the other hand, it is known that the *stratum corneum* acts as a barrier to hydrophilic and ionized-species movement and, consequently, represent the biggest resistive portion of the skin-electrode interface impedance. However, when wet, sweaty or bypassed, the conductance of the *stratum corneum* increases considerably [15].

It is documented that the body impedance during transcutaneous stimulation undergoes non-linear variations [19], which are mainly attributed to the skin-electrode interface. Some studies have localized this phenomenon in the *stratum corneum*, and showed a significant reduction of such variability, when this layer is removed [10,21,22].

Once the electrode-electrolyte exchange occurs in the electrode (between the conductive material and an electrolyte solution, *e.g.* hydrogel), the ionic flow has at least two pathways into the *stratum corneum*: the first one that goes between the stratification of the corneocyte matrix layers; and a second one that goes through the appendages, mainly the sweat macropores (Fig 1). It has been shown that most of the ionic movement happens in the sweat pores, since the sweat is an electrolytic fluid and highly conductive [20].

Impedance variation mechanisms. There are many theories that try to explain the mechanisms that underlay the impedance variations on the skin. In a general sense, all of them describe structural changes that increase the ease of the electrical current to flow through the tissue, also known as conductivity (inverse of the resistance). The theories about how conductivity changes can be grouped according to the speed of the mechanisms that describe: instantaneous changes (within few microseconds [16,18,23]) and progressive changes (from milliseconds up to hours [2,10,23,24]).

The instantaneous changes are commonly addressed to the electroporation of the skin, which is the phenomenon where the membrane permeability to ions and macromolecules is increased by exposing it to a high electrical field (Fig 1) [25]. For transcutaneous electrical stimulation, the electroporation process occurs in both ionic pathways (matrix and pores), but at low amplitudes just the macropores are affected. This is because the lipid-corneocyte matrix is composed by multiple layers; therefore the electric potential drop in each layer is a small fraction of the applied voltage. On the other hand, macropores are composed only by few layers; therefore the potential drop across each layer is higher.

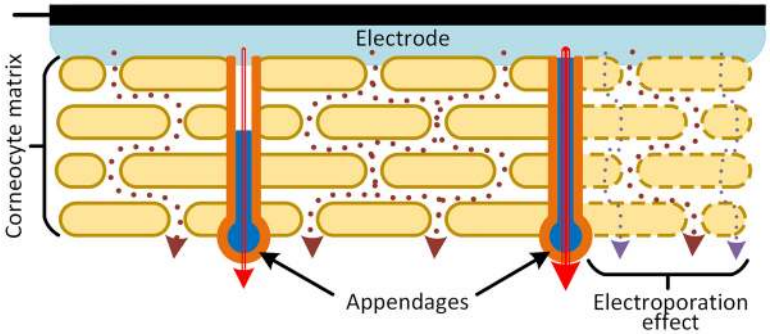

Fig 1. Simplify model of the skin-electrode interface, the stratum Corneum and its ionic pathways. Pathways in the appendages are shown in hard lines, and pathways going between the stratification of the *stratum corneum* matrix are shown in dotted lines. The electroporation effect on the corneocyte matrix is shown at the right, while the current flow increase due to the pore filling is shown in the appendages. Adapted from [2,5,11,20].

doi:10.1371/journal.pone.0125609.g001

While instantaneous impedance variations have been widely investigated, there is still controversy about the mechanism of the slow changes. The most extended studies suggest that progressive increase of ions in the interface could be the answer [2,5,24]. Almasi & Schmitt concluded that impedance reduction in long-term applications is mainly related to the skin below the electrode getting increasingly hydrated or wet. This is due to the natural diffusion of ions and the expelled sweat that remains trapped below the electrode [24]. However these mechanisms work in the time scale of seconds up to hours and cannot explain the non-exponential behavior of the impedance within the duration of the electrical pulses. Grimnes and collaborators have proposed electro-osmosis and/or electrophoresis as mechanisms for ion movement, specifically for filling up the sweat conducts [2,5]. Both mechanisms are suitable to explain the impedance variations within the duration of the stimulus, since they start to work instantaneously and change along the pulse depending on the injected charge and speed of ions in the medium. The impedance variation due to the filling of sweat-pores (appendages) is represented in Fig 1, where bigger currents cross through the completely filled ducts rather than in the semi-filled ducts.

Mathematical model

The developed mathematical model is based on two assumptions:

1. The electroporation effect is instantaneous, since the transient (few microseconds) cannot be detected at the sampling rate used.
2. The impedance of the deep-tissue and the bulk solution of the electrode remain constant for each subject.

Due to the complexity of the skin-electrode interface, impedance measurements cannot be done directly. Instead, an equivalent RC-network model can be used and tuned to describe the measured current-voltage response [19,26]. A widely use equivalent network is shown in Fig 2b, but many other models can be found in literature [2,3,9,10,19,21,27,28]. A modification of the model presented by Chizmadzhev *et al.* is shown in Fig 2a as a detailed model of the system [17]. In this full model, the bulk resistance of the electrolyte in the electrode (R_b) and the tissue (R_t) are presented separately. Also, both ionic pathways of the *stratum corneum* are considered with R_{me} and C_m for the lipid-corneocyte matrix, and R_{ae}, R_{ao} and C_a for the skin appendages. Notice that the suffixes *e* and *o* stand for electroporation and charge-dependent (presumably electro-osmosis) effects respectively. Since the time constant for the lipid-corneocyte matrix is less than 1μs [17], the capacitor C_m is fully charged before the first sampling. Therefore C_m can be considered as an open-circuit and discarded from the model. Because R_b and R_t are constant and inherent to the system, they can be merged into a series resistance R_s.

R_{ao} represents the resistance in the skin appendages when they are not completely filled with electrolyte. If the cases are considered, where the skin is fully wet or the charge-dependent effect is saturated (high pulse charges), then R_{ao} converges towards zero ($R_{ao}\rightarrow 0$), and the resultant parallel resistance R_e ($R_{me} \parallel R_{ae}$) is defined by the impedance variations due to the electroporation of both ionic pathways (Fig 2b). Such simplification can be also applied to low charge impulses, where the charge-dependence becomes negligible and R_{ao} can be integrated as a constant in R_e. In order to keep the duality for low and high charge pulses, the model shown in Fig 2c is proposed. Notice that the two resistances of the skin are placed in series instead of parallel (as should follow from Fig 2a), because the resulting values for a parallel model ($R_{me} \parallel R_{ae}$ and R_{ao}) would lead to very high values. Otherwise, the proposed model shows similar values as to be found in literature.

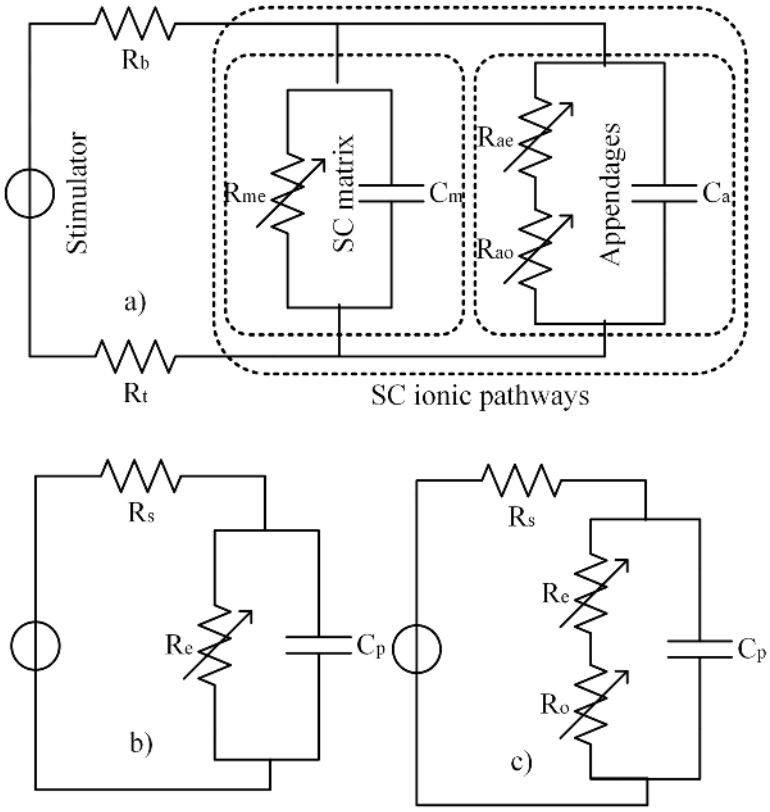

Fig 2. Skin-Electrode interface models. a) Full model considering electroporation and a charge-dependent effect; b) Simple model for low charge pulses; c) Proposed model.

doi:10.1371/journal.pone.0125609.g002

The physiological phenomenon induced by electroporation is described as an increase of the tissue conductance G_e. Preliminary data suggest that such changes can be modeled with a linear equation describing the course of G_e in dependence of the stimulation current as in Eq (1) [11]. This assumption leads to a R_e model similar to an initial exponential decay, which is consistent with other work to be found in literature [19].

$$\begin{aligned} R_e &= \frac{1}{G_e} \\ G_e(S) &= a_e S(t) + b_e \end{aligned} \tag{1}$$

Where $S(t)$ represents the stimulation current at a given time (t), b_e is the conductance at no excitation ($S = 0\text{mA}$), and a_e defines the conductance increase with respect to the current.

In contrast to the fast reacting electroporation, the electro-osmosis related flow rate into a semi-filled capillary is described as a function of the electro-kinetic potential and medium properties [5]. It is limited by the channel lumen and the repelling diffusion force generated by the electrolyte concentration increase near the electrode interface. In the final model, the charge-dependent effect (R_o) goes from an initial value (given for typical skin conditions)

down to zero, when the skin is completely humid.

$$R_o = \begin{cases} R_{oi} & , Ch < ACh_{th} \\ R_{oi}\left(1 - \dfrac{1}{1 + \dfrac{Aa_o}{Ch(t) - ACh_{th}}}\right) & , Ch \geq ACh_{th} \end{cases} \quad (2)$$

$$R_{oi} = R_p(t = 0) - \mathrm{R}_e \quad (3)$$

$$Ch(t) = \sum_{t=0}^{t} |i(t)| T_s \quad (4)$$

$$a_o = a_a I(t) + b_a \quad (5)$$

Where R_{oi} is the initial resistance that depends on the skin conditions, A is the electrode area in cm^2, Ch_{th} is the charge threshold, where the electro-osmotic effect starts to be relevant (inflexion point) in [C/cm^2], $Ch(t)$ represents the charge of the pulse at time t, T_s is the sampling period and a_o is the variation of the electrical properties of the medium due to electroporation.

The equivalent RC model shown in Fig 2c follows, under typical conditions, the step response described by Eqs (6) and (7) for CC and VC respectively [29].

$$v(t) = i(t)R_s + i(t)R_p\left(1 - e^{-\frac{t}{R_p C}}\right) \quad (6)$$

$$i(t) = \frac{v(t)}{R_s + R_p} - \left(\frac{v(t)}{R_s + R_p} - \frac{v(t)}{R_s}\right) e^{-\frac{t}{(R_s \| R_p) C}} \quad (7)$$

$$R_p = \mathrm{R}_e + R_o = \frac{1}{G_p} \quad (8)$$

$$G_p(S) = a_p S(t) + b_p \quad (9)$$

For both cases, the evaluation of the voltage-current response at t = 0 reflects the value of R_s, because the capacitor acts as short-circuit. On the other hand, the final stable value corresponds to the relation of R_s and R_p, because a fully-charged capacitor behaves as an open circuit. Notice also that if enough charge is applied (*e.g.* at the end of the pulse), then R_o converges to zero ($R_o \rightarrow 0$) and R_p will depict the value of R_e. R_p and C were estimated through a fitting based on Eqs (6) and (7) applied to the signal below Ch_{th}. Similar to R_e, R_p was modeled with a linear increasing of its conductance G_p as in Eq (9).

In order to model the dependence of a_o to the electroporation, stimulus amplitude was adjusted to different CC levels and then fitted with a linear regression based on Eq (5).

Experimental Setup

A total of ten measurements sessions were considered. The protocol was approved by the Ethics in Research Committee and the Research Committee of the School of Medicine of the Tecnológico de Monterrey (Mexico), and conducted according to the principles of the Helsinki Declaration. A total of five neurological-intact volunteers participate in this experiment and all were informed of the experimental procedure, benefits and potential risks of the measurements, and

signed an informed consent prior the measurements. The protocol included application of electrical stimulation on both legs of each volunteer. CC and VC stimulation were applied using commercial self-adhesive hydrogel electrodes (SN-50900, Hivox Biotek Inc., Taiwan) of two sizes: 5x10cm (ETD) and 5x5cm (ETC). For both CC and VC stimulation the stimulator output stage STMISOLA (Biopac Systems, Inc., USA) controlled via NI MyDAQ card (National Instruments, Inc., USA) was used. The electrical stimulation was applied to the anterior thigh (anodic electrode proximally) with an inter-electrode distance of 10cm. A custom code was implemented in LabView 2012 (National Instruments, Inc., Ireland) to control both the stimulator and the acquisition of the voltage-current response (sample rate 150kS/s).

The whole protocol was based on charge-balanced biphasic rectangular pulses and consisted of four stages: CC with the bigger electrodes (ETD), VC with ETD, CC with smaller electrodes (ETC) and, VC with ETC. The stimulation sweeps were done at 30,000μs per phase and varied from 1mA or 1V (in steps of 1mA or 1V) up to the pain threshold of the individual subject or the upper current limit of the stimulator (110mA).

Data Processing

The data were post-processed in MATLAB (The MathWorks, Inc., USA). The acquired data were filtered with a moving average filter (span = 5) and an offset extraction on both signals was performed. Afterward, four time points were detected (Fig 3):

1. Beginning of the pulse (t_{i1}): for CC, it is the time when the first current sample is equal or greater than the 99% of the pulse amplitude. For VC it is the time when the peak current sample appears with the leading impulse edge.
2. End of first phase (t_{f1}): It is the time when first sample (after t_{i1}) falls below 99% of the pulse amplitude in the first trailing edge.

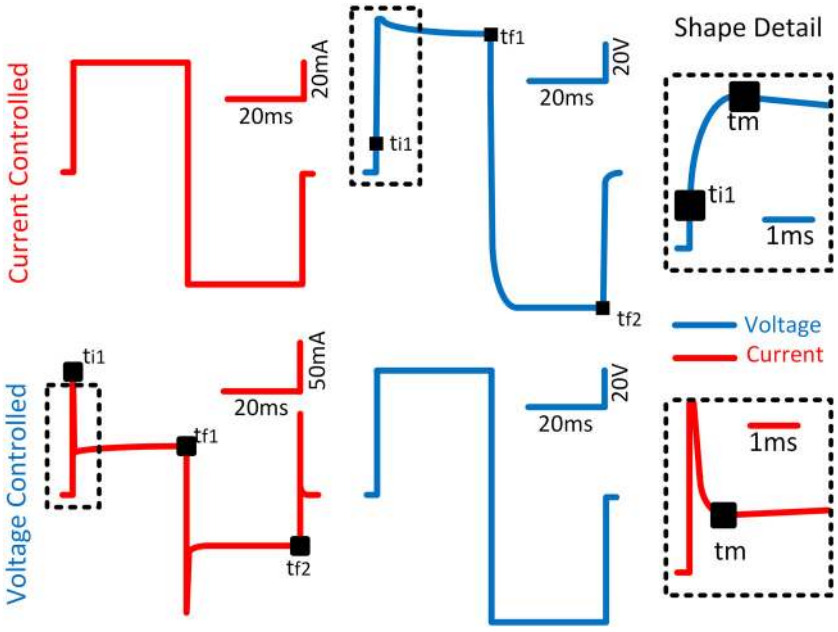

Fig 3. Representation of the current-voltage response during CC (top) and VC (down) with biphasic pulses of 30ms per phase. A detail of the first milliseconds is displayed for better appreciation of the inflexion point and the beginning of the pulse.

doi:10.1371/journal.pone.0125609.g003

3. End of second phase (t_{f2}): It is the time when the last current sample (after t_{f1}) remains below -99% of the pulse amplitude.

4. Inflexion point (t_m): It is the time when the electro-osmotic effect starts modifying the exponential trace expected from RC circuit model calculations, which is defined as Ch_{th}.

R_s and R_e were calculated from the apparent impedance at t_{i1} and t_{f2} (if stability is reached) respectively. The applied charge at the time points t_m, t_{f1} and t_{f2} was calculated with Eq (4). Finally, C and R_p were estimated with Eqs (6) and (7) using the time segments where the applied charge was below Ch_{th}. Time reference was the initiation of the leading impulse edge by the control input.

Evaluation

In order to validate the model, a virtual bench was developed on Simulink (The MathWorks, Inc., USA). While the model was fitting mostly with the data from the first phase of the impulse, the simulation was done along the entire impulse. Then, the R^2 and MSE values for the simulation were calculated.

Results

The values of R_s remain quasi-stable along the whole stimulation amplitude variation range. A slight decreasing trend was observed in some cases, however, within practical stimulation intensity ranges, this decreasing can be considered as negligible. Table 1 presents the R_s values for each electrode size and each stimulus type (Mean±SD).

An exemplary result of R_e values (one subject) in relation to the current and voltage at t_{f2} is shown in Fig 4. The consistency of values in relation with the current, unlike the voltage, speaks for a current-dependence to the electroporation effect. Table 2 shows the average values of the coefficients for G_e estimation, and the R^2 of the fitting.

The inflexion point was easier to detect in VC pulses, where the charge injection is small and the charge-dependent effect appears progressively in the recorded traces. For CC impulses on the other hand, due to the fast charge injection, the detection of the inflexion point was not possible because only one measurement per subject (1mA with big electrodes) did not show the charge-dependent effect. The charge threshold average at small amplitudes was 350nC/cm^2 and was similar for all subjects. High amplitude pulses were not considered since the huge current peak dynamic biased the detection to bigger values (~402nC/cm^2).

Once the beginning of the charge-dependent effect was defined, an estimation of the current-voltage response was done with the data preceding the Ch_{th} (Fig 5). Such estimation provides the C values shown in Table 1, as well as R_p and the error induced by the charge-dependent effect.

Table 1. Summary of estimated R_s and C values.

Variable	Stimulation Type	50cm^2	25cm^2
R_s	CC	498±83Ω	670±99Ω
	VC	440±60Ω	596±86Ω
C	CC	194±52nF	106±25nF
	VC	176±62nF	83±31nF

Summary for all subjects of the R_s and C values based on the stimulation type and electrode size.

doi:10.1371/journal.pone.0125609.t001

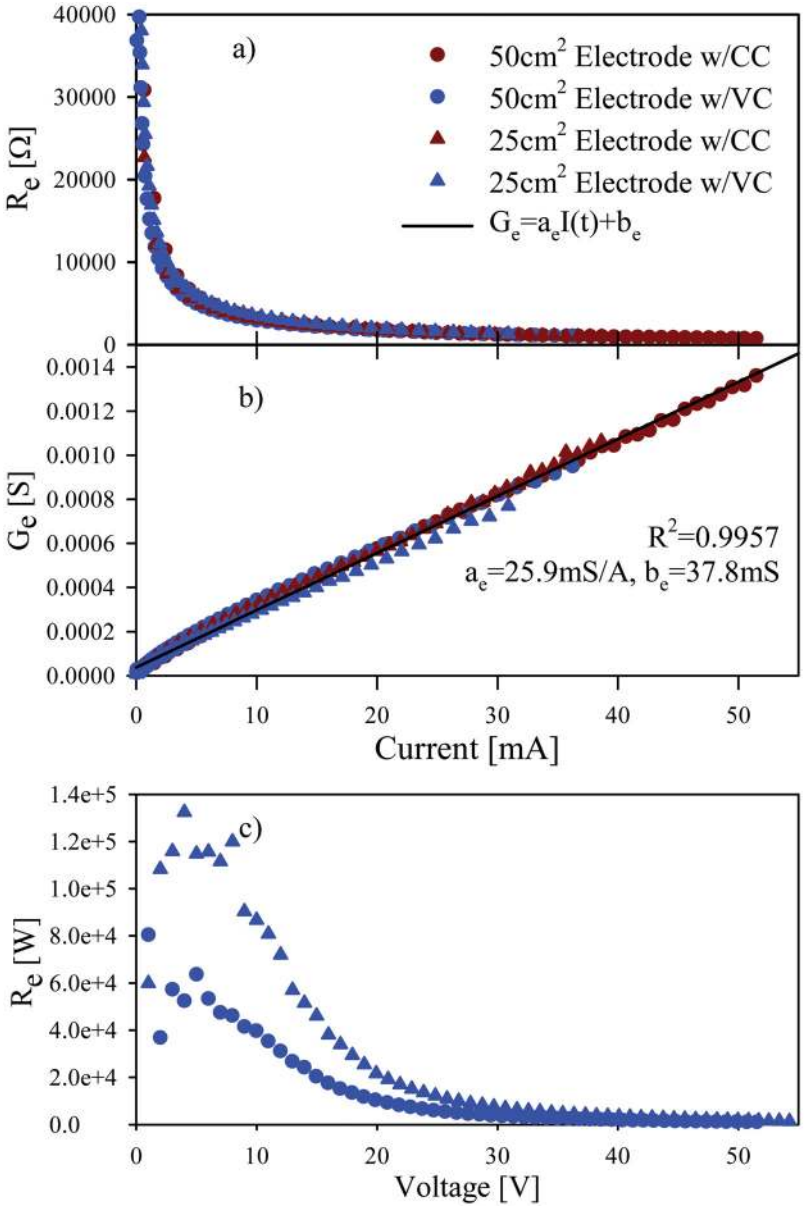

Fig 4. Typical estimated R_e values as function of a) current and c) voltage. b) G_e values as function of the current.

doi:10.1371/journal.pone.0125609.g004

Table 2. Summary of values to estimate G_e and G_p.

Conductance	Coefficient	mean±SD	Range
	a_e	24±4mS/A	18–30mS/A
G_e	b_e	64±30μS/A	14–104μS/A
	R^2	0.979	0.956–0.997
	a_p	14±3.5mS/A	7.6–19mS/A
G_p	b_p	56±33μS	7.8–109μS
	R^2	0.939	0.866–0.982

Summary of the coefficients required to estimate G_e and G_p for all the subjects.

doi:10.1371/journal.pone.0125609.t002

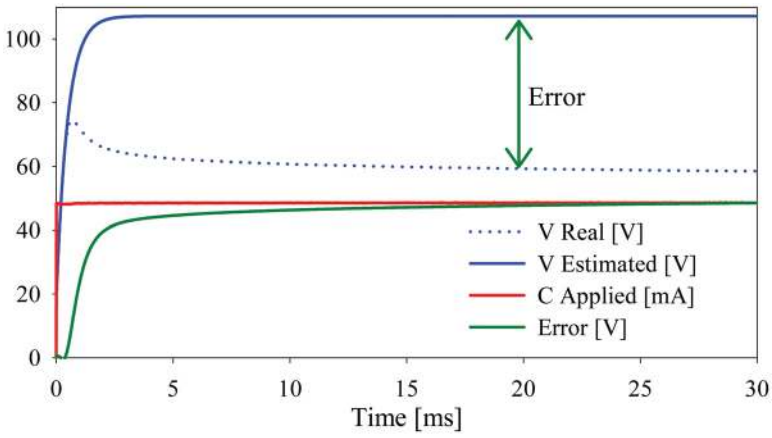

Fig 5. Typical voltage response estimation without considering the charge-dependent effect.

doi:10.1371/journal.pone.0125609.g005

G_p was modeled on basis of its linear dependence from current amplitude (Fig 6). It is important to notice that for VC stimulation the current at steady state was used as reference. The coefficients to estimate G_p are shown in Table 2. Finally, based on G_e and G_p estimation, R_{oi} was calculated based on Eq (3). The coefficient values for subject 9 (used example in all the figures) are summarized in Table 3.

Simulation was done for all pulses in CC and VC for both electrode sizes. Exemplary results are shown in Fig 7 along with the mean square error (MSE) and R^2 of each impulse.

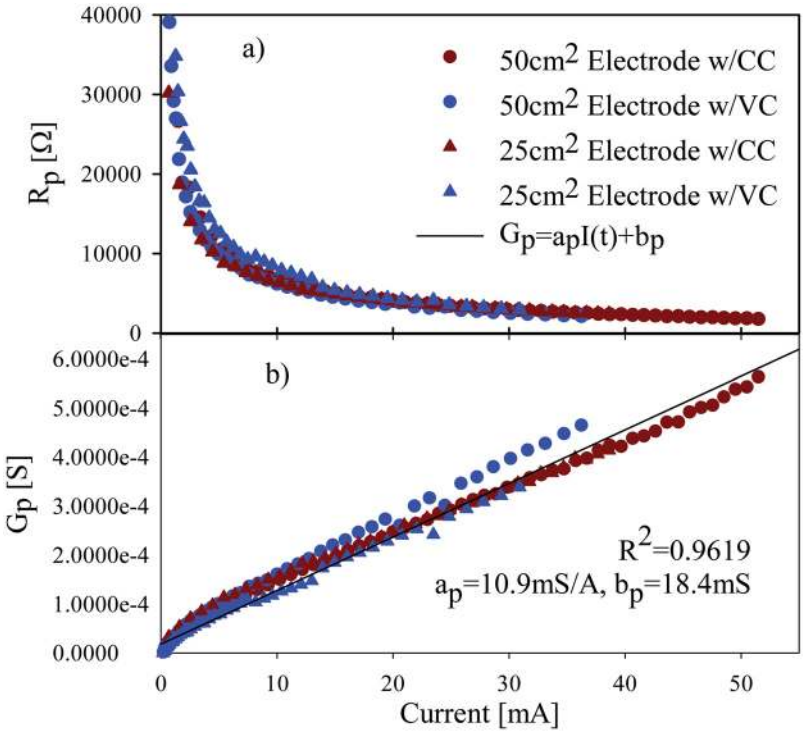

Fig 6. a) Typical estimated R_p values as function of current and; b) G_p values as function of the current.

doi:10.1371/journal.pone.0125609.g006

Table 3. Coefficient values for Subject 9.

Symbol	Value	Units
R_s (50cm^2)	CC:387,VC:356	Ω
R_s (25cm^2)	CC:515,VC:481	Ω
C (50cm^2)	CC:269,VC:259	nF
C (25cm^2)	CC:139,VC:117	nF
Ch_{th}	350	nC/cm^2
a_p	10.9	mS/A
b_p	18.4	μS
a_e	25.9	mS/A
b_e	37.8	μS
a_a	4000	nC/(A·cm^2)
b_a	70	nC/cm^2

Summary of the required coefficients to implement the model specifically fitted for subject 9, which was used as an example in all the figures.

doi:10.1371/journal.pone.0125609.t003

Discussion

The slight decreasing trend of R_s values suggests that the electrical field induced in an organism leads to electroporation also in deeper lying tissue. As expected, the electroporation of deeper lying tissue is considerably smaller because of dispersion and attenuation of field strengths, but even more pronounced due to the low electrical resistance of the deeper tissue layers with smaller voltage drop in comparison to higher impedance layers at the surface (voltage divider effect). Additionally, differences between estimated values for CC and VC were noticed. It is possible that the measured differences are influenced by the assumption of an ideal pulse intensity step. For this reason, especially for CC mode, deviations in the initial resistance value could be originated by the capacitor charge at the moment of the first sample. However, the stability of the measurement is noticed in the consistent higher resistances values of the small electrodes, and a normal inter-individual variation range of resistance values.

The capacitance was modeled as a constant within all stimulation intensity ranges. As in R_s, a slightly decreasing trend was observed in some cases. However, such decrease can be neglected since no relevant improvement was obtained in the accuracy of the final model when a variable capacitance was considered. In general, the capacitance of the big electrodes appeared as about twice the small ones, which directly correlates with the size relations and speaks for a proper estimation.

The estimation of R_p was done on bases of a current-dependence assumption. The linear model was fitting well, but like R_e, the model cannot describe the entire control characteristic, since the value of the conductance (G_p) must saturate in some point, which cannot be explored with the actual setup. Although the model lacks considering high intensity scenarios, it predicts essentially the entire clinically applicable amplitude ranges for intact skin sensation. Since the stimulation was performed below the pain threshold of the volunteers the outcome does not represent higher intensities as applicable in *e.g.* sensory complete spinal cord injured people.

The coefficient a_o was adjusted to give more weight to the beginning of each phase (and less to the saturating values towards the end). Since it is assumed that the charge-dependence is based on ion movement the electrical field, the current-dependence of a_o is also consistent with the change of the medium resistivity likely caused by the electroporation.

Although the model is based mainly on parameters fitted to the first phase, the dynamic simulation shows that it is able to predict the impedance behavior during both phases of the

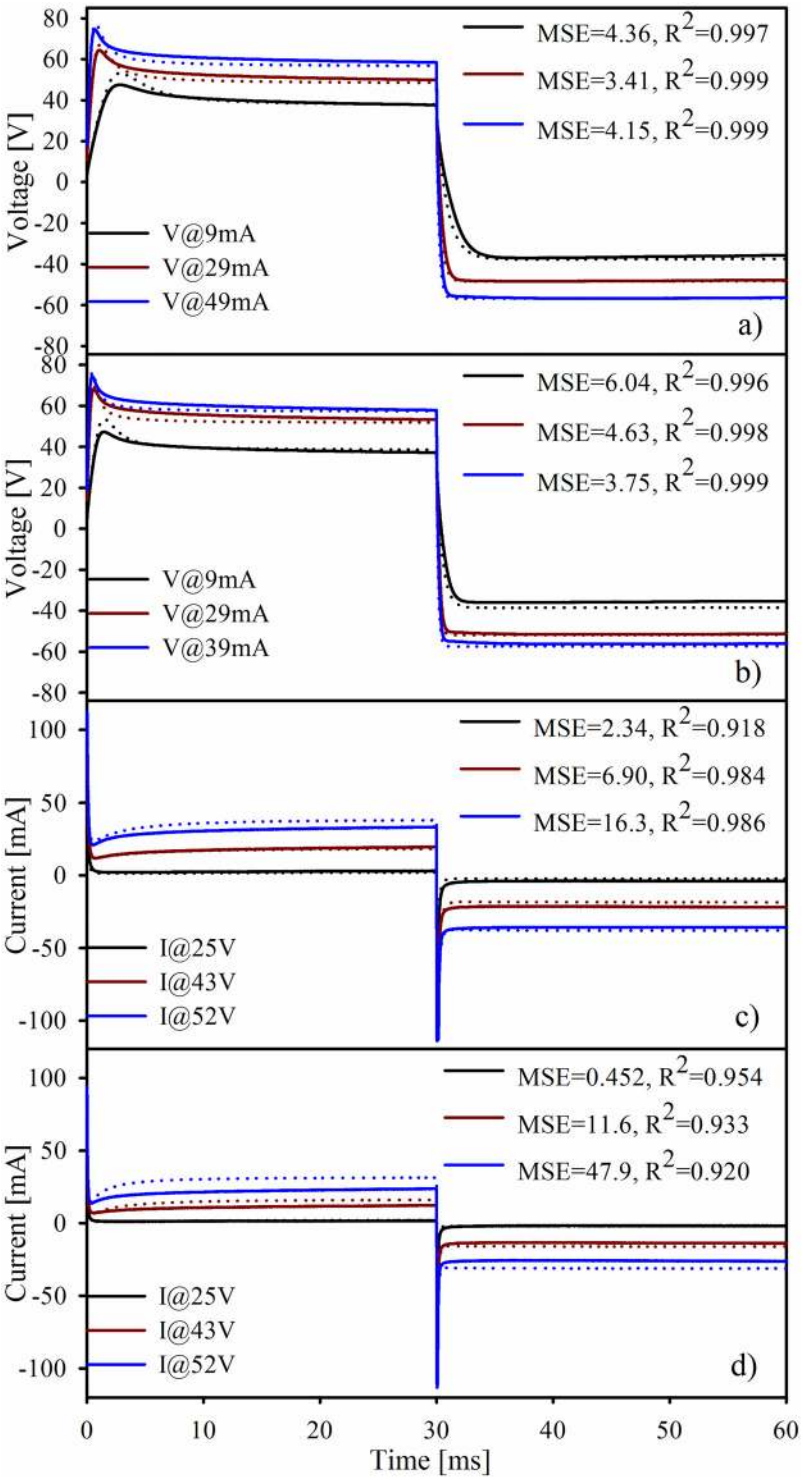

Fig 7. Comparison of exemplary measured values (hard line) and the simulation results (dotted lines) for a) CC with ETD, b) CC with ETC electrodes, c) VC with ETD and, d) VC with ETC.

doi:10.1371/journal.pone.0125609.g007

pulse with good correlation. It also is able to deal with different electrode sizes and stimulation control type. The R^2 and MSE remain in acceptable levels in CC while in VC these parameters appear slightly degraded presumably because of small mismatches in the saturation levels.

Various mathematical models are presented in literature describing different applications and setups of electrical stimulation. However, most of them do not consider the variability of the skin impedance that, as shown in this work, may considerably change between pulses and within the pulse duration. The work presented here can be applied to larger electrical stimulation models either for pulse shape optimization or studying the viability of novel stimulation techniques. For example, Krouchev and colleges present a general mathematical model to design an energy-optimal electrical impulse for activating nerve fibers [30]. Based on this work, an extended model could be developed that includes transcutaneous electrode based applications, where the skin impedance plays an important role [1]. Danner and colleges developed a computer simulation to assess viability of transcutaneous spinal cord stimulation as an alternative to epidural stimulation [31]. In their work the skin impedance was considered constant, inclusion of the now presented interface model might lead to further refinement of the simulation, validity of interpretation and optimization of the stimulus parameters. The further achievement of the presented model could be in interpretation of the effects of subthreshold stimulus *e.g.* pre-conditioning pulses. It has been shown that pre-conditioning pulses may increase or decrease the fibers excitability [32], when applied transcutaneously such pre-pulses may substantially reduce the skin-electrode impedance. Therefore, the impedance reduction may play a secondary effect, which magnitude should be quantified.

Conclusions

The proposed model is able to describe the skin-electrode interface impedance dynamically for different electrode sizes, with the same construction, and different stimulation modes (CC and VC). The mathematical model is based on the anatomical structure of the interface zone and its variables represent a biological phenomenon and structure.

The whole model is based on nine variables. With exception of R_s and C, all variables can be calculated from recordings along a single sweep of stimulation amplitudes and are valid for different electrode sizes and stimulation modes. R_s and C, on the other hand, must be calculated for each electrode configuration separately. It is important to notice that G_e, G_p and a_o are modeled with a linear approach, therefore, only few points are required for its calculation, while R_s, C and Ch_{th} require, essentially, only one reference point.

Unlike other works found in literature, this model is developed using typical stimulation parameters for clinical applications of transcutaneous electrical stimulation: pulse waveforms, stimulation amplitude ranges and stimulus duration. In the latter case, although the long durations are specifically necessary for activation of denervated muscles fibers, the impedance behavior is also directly relevant for shorter pulses, as applied for nerve stimulation, since it is identical in the initial phase of the impulse, independently from the further impulse duration.

The whole model is current-based, and it can be dynamically adjusted. This allows the predictive modelling of current-voltage responses for vastly any impulse and, therefore, the performance analysis and optimization of new pulse waveforms and stimulation techniques.

Author Contributions

Conceived and designed the experiments: JLVL MK. Performed the experiments: JLVL. Analyzed the data: JLVL WM. Contributed reagents/materials/analysis tools: JLVL JACR. Wrote the paper: JLVL MK JACR WM.

References

1. Vargas Luna JL, Krenn M, Cortés JA, Mayr W (2013) Comparison of Current and Voltage Control Techniques for Neuromuscular Electrical Stimulation in the Anterior Thigh. Biomed Tech (Berl) 58. Available: http://www.scopus.com/inward/record.url?eid=2-s2.0-84903954715&partnerID=tZOtx3y1. Accessed 9 January 2015.
2. Grimnes S (1983) Skin impedance and electro-osmosis in the human epidermis. Med Biol Eng Comput 21: 739–749. Available: http://www.springerlink.com/index/10.1007/BF02464037. Accessed 29 January 2013. PMID: 6664134
3. Franks W, Schenker I, Schmutz P, Hierlemann A (2005) Impedance characterization and modeling of electrodes for biomedical applications. IEEE Trans Biomed Eng 52: 1295–1302. Available: http://www.ncbi.nlm.nih.gov/pubmed/16041993. PMID: 16041993
4. Schwan HP (1968) ELECTRODE POLARIZATION IMPEDANCE AND MEASUREMENTS IN BIOLOGICAL MATERIALS. Ann N Y Acad Sci 148: 191–209. Available: doi: 10.1111/j.1749-6632.1968.tb20349.x. Accessed 6 February 2014. PMID: 5237641
5. Johnsen GK, Lütken C a, Martinsen ØG, Grimnes S (2011) Memristive model of electro-osmosis in skin. Phys Rev E 83: 031916. Available: doi: 10.1103/PhysRevE.83.031916. Accessed 16 May 2013. PMID: 21517534
6. Krenn M, Haller M, Bijak M, Unger E, Hofer C, Kern H (2011) Safe neuromuscular electrical stimulator designed for the elderly. Artif Organs 35: 253–256. Available: http://www.ncbi.nlm.nih.gov/pubmed/21401669. Accessed 30 October 2013. doi: 10.1111/j.1525-1594.2011.01217.x PMID: 21401669
7. Hofer C, Mayr W, Stöhr H, Unger E, Kern H (2002) A stimulator for functional activation of denervated muscles. Artif Organs 26: 276–279. Available: http://www.ncbi.nlm.nih.gov/pubmed/11940032. PMID: 11940032
8. Birlea SI, Birlea NM, Breen PP (2008) Identifying Skin Electrical Properties Using a Standard Neuro-Muscular Electrical Stimulation Voltage Pulse. Signals and Systems Conference, 208. (ISSC 2008). IET Irish. Galway, Ireland. pp. 55–59.
9. Kantor G, Alon G, Ho HS (1994) Simulated tissue loads for testing of transcutaneous electrical stimulators. Proceedings of 16th Annual International Conference of the IEEE EMBS. IEEE. pp. 784–785. Available: http://ieeexplore.ieee.org/lpdocs/epic03/wrapper.htm?arnumber=415291. Accessed 23 November 2012.
10. Dorgan SJ, Reilly RB (1999) A model for human skin impedance during surface functional neuromuscular stimulation. IEEE Trans Rehabil Eng 7: 341–348. Available: http://www.ncbi.nlm.nih.gov/pubmed/10498379. PMID: 10498379
11. Luna JLV, Krenn M, Ramírez JAC, Mayr W (2014) Skin-Electrode Impedance Model for Typical Transcutaneous Electrical Stimulation Pulses. Proceedings of the IASTED International Conference on Biomedical Engineering, BioMed 2014. Calgary,AB, Canada: ACTAPRESS. pp. 190–195. Available: http://www.scopus.com/inward/record.url?eid=2-s2.0-84906979378&partnerID=tZOtx3y1. Accessed 5 January 2015.
12. Vargas Luna JL, Krenn M, Cortes Ramirez JA, Mayr W (2014) Use of an Inter-Phase Pause to Increase the Efficiency of Biphasic Pulses on Transcutaneous Electrical Stimulation. Biomed Tech (Berl) 59: 1045–1048. doi: 10.1515/bmt-2014-5013
13. Grill WM, Mortimer JT (1995) Stimulus waveforms for selective neural stimulation. IEEE Eng Med Biol Mag 14: 375–385. Available: http://ieeexplore.ieee.org/lpdocs/epic03/wrapper.htm?arnumber=395310.
14. Tortora GJ, Reynolds Grabowski S (2002) Principios de Anatomía y Fisiología. 7th ed. Mexico D.F.: Oxford México.
15. Reilly JP (1992) Electrical Stimulation and Electropathology. 1st. Editi. New York, USA: Cambridge University Press.
16. Chizmadzhev YA, Zarnitsin VG, Weaver JC, Potts RO (1995) Mechanism of electroinduced ionic species transport through a multilamellar lipid system. Biophys J 68: 749–765. Available: http://www.pubmedcentral.nih.gov/articlerender.fcgi?artid=1281799&tool = pmcentrez&rendertype = abstract. Accessed 26 November 2013. PMID: 7756542
17. Chizmadzhev YA, Indenbom A V, Kuzmin PI, Galichenko S V, Weaver JC, Potts RO (1998) Electrical properties of skin at moderate voltages: contribution of appendageal macropores. Biophys J 74: 843–856. Available: http://www.pubmedcentral.nih.gov/articlerender.fcgi?artid=1302564&tool = pmcentrez&rendertype = abstract. Accessed 15 March 2013. PMID: 9533696
18. Pliquett U, Langer R, Weaver JC (1995) Changes in the passive electrical properties of human stratum corneum due to electroporation. Biochim Biophys Acta—Biomembr 1239: 111–121. Available: http://linkinghub.elsevier.com/retrieve/pii/000527369500139T. Accessed 27 June 2013.

19. Keller T, Kuhn A (2008) Electrodes for transcutaneous (surface) electrical stimulation. J Autom Control 18: 35–45. Available: http://www.doiserbia.nb.rs/Article.aspx?ID=1450-99030802035K. Accessed 12 March 2013.
20. Grimnes S (1984) Pathways of ionic flow through human skin in vivo. Acta Derm Venereol 64: 93–98. Available: http://www.ncbi.nlm.nih.gov/pubmed/6203315. PMID: 6203315
21. Boxtel A (1977) Skin resistance during square-wave electrical pulses of 1 to 10 mA. Med Biol Eng Comput 15: 679–687. Available: http://www.springerlink.com/index/10.1007/BF02457927. Accessed 29 January 2013. PMID: 203791
22. Lykken DT (1970) SQUARE-WAVE ANALYSIS OF SKIN IMPEDANCE. Psychophysiology 7: 262–275. Available: doi: 10.1111/j.1469-8986.1970.tb02232.x. Accessed 9 May 2013. PMID: 5499129
23. Jadoul A, Bouwstra J, Préat V (1999) Effects of iontophoresis and electroporation on the stratum corneum. Adv Drug Deliv Rev 35: 89–105. Available: http://linkinghub.elsevier.com/retrieve/pii/S0169409X98000659. Accessed 27 June 2013. PMID: 10837691
24. Almasi JJ, Schmitt OH (1970) SYSTEMIC AND RANDOM VARIATIONS OF ECG ELECTRODE SYSTEM IMPEDANCE. Ann N Y Acad Sci 170: 509–519. Available: doi: 10.1111/j.1749-6632.1970.tb17718.x. Accessed 23 January 2013.
25. Ivorra A (2010) Tissue electroporation as a bioelectric phenomenon: Basic concepts. In: Rubinsky B, editor. Irreversible Electroporation. Springer Berlin Heidelberg. pp. 23–61. Available: http://link.springer.com/chapter/10.1007/978-3-642-05420-4_2. Accessed 28 November 2013.
26. Lykken DT, Venables PH (1971) Direct measurement of skin conductance: a proposal for standardization. Psychophysiology 8: 656–672. Available: http://www.ncbi.nlm.nih.gov/pubmed/854561. Accessed 18 March 2013. PMID: 5116830
27. Lackermeier A, Pirke A, McAdams ET, Jossinet J (1996) Non-linearity of the skin's AC impedance. Proceedings of 18th Annual International Conference of the IEEE Engineering in Medicine and Biology Society. Amsterdam: IEEE, Vol. 5. pp. 1945–1946. Available: http://ieeexplore.ieee.org/lpdocs/epic03/wrapper.htm?arnumber=646332. Accessed 10 May 2013.
28. Chen C-F, Chen W-S, Chou L-W, Chang Y-J, Chen S-C, Kuo T-S, et al. (2012) Pulse energy as a reliable reference for twitch forces induced by transcutaneous neuromuscular electrical stimulation. IEEE Trans neural Syst Rehabil Eng 20: 574–583. Available: http://www.ncbi.nlm.nih.gov/pubmed/22481833. doi: 10.1109/TNSRE.2012.2188305 PMID: 22481833
29. Glisson TH (2011) Introduction to Circuit Analysis and Design. Dordrecht: Springer Netherlands. Available: http://www.springerlink.com/index/10.1007/978-90-481-9443-8. Accessed 5 March 2013.
30. Krouchev NI, Danner SM, Vinet A, Rattay F, Sawan M (2014) Energy-optimal electrical-stimulation pulses shaped by the least-action principle. PLoS One 9: e90480. Available: http://www.pubmedcentral.nih.gov/articlerender.fcgi?artid=3953645&tool = pmcentrez&rendertype = abstract. Accessed 26 March 2014. doi: 10.1371/journal.pone.0090480 PMID: 24625822
31. Danner SM, Hofstoetter US, Ladenbauer J, Rattay F, Minassian K (2011) Can the human lumbar posterior columns be stimulated by transcutaneous spinal cord stimulation? A modeling study. Artif Organs 35: 257–262. Available: http://www.ncbi.nlm.nih.gov/pubmed/21401670. Accessed 16 July 2014. doi: 10.1111/j.1525-1594.2011.01213.x PMID: 21401670
32. Grill WM, Mortimer JT (1996) The effect of stimulus pulse duration on selectivity of neural stimulation. IEEE Trans Biomed Eng 43: 161–166. Available: http://www.ncbi.nlm.nih.gov/pubmed/8682527. PMID: 8682527